

Submillimetre observations of *WISE*-selected high-redshift, luminous, dusty galaxies

Suzy F. Jones,^{1*} Andrew W. Blain,¹ Daniel Stern,² Roberto J. Assef,³
Carrie R. Bridge,⁴ Peter Eisenhardt,² Sara Petty,⁵ Jingwen Wu,⁶
Chao-Wei Tsai,² Roc Cutri,⁷ Edward L. Wright⁶ and Lin Yan⁷

¹University of Leicester, X-ray and Observational Astronomy Group (XROA), Department of Physics & Astronomy, University Road, Leicester LE1 7RH, UK

²Jet Propulsion Laboratory, California Institute of Technology, 4800 Oak Grove Dr., Pasadena, CA 91109, USA

³Núcleo de Astronomía de la Facultad de Ingeniería, Universidad Diego Portales, Av. Ejército Libertador 441, Santiago, Chile

⁴California Institute of Technology MS249-17, Pasadena, CA 91125, USA

⁵Virginia Polytechnic Institute & State University, Department of Physics MC 0435, 850 West Campus Drive, Blacksburg, VA 24061, USA

⁶Division of Physics & Astronomy, University of California Los Angeles, Physics and Astronomy Building, 430 Portola Plaza, Los Angeles, CA 90095-1547, USA

⁷Infrared Processing and Analysis Center, California Institute of Technology, MS 100-22, Pasadena, CA 91125, USA

Accepted 2014 June 9. Received 2014 June 2; in original form 2014 January 24

ABSTRACT

We present SCUBA-2 (Submillimetre Common-User Bolometer Array) 850 μm submillimetre (submm) observations of the fields of 10 dusty, luminous galaxies at $z \sim 1.7\text{--}4.6$, detected at 12 and/or 22 μm by the *Wide-field Infrared Survey Explorer* (*WISE*) all-sky survey, but faint or undetected at 3.4 and 4.6 μm ; dubbed hot, dust-obscured galaxies (Hot DOGs). The six detected targets all have total infrared luminosities greater than $10^{13} L_{\odot}$, with one greater than $10^{14} L_{\odot}$. Their spectral energy distributions (SEDs) are very blue from mid-infrared to submm wavelengths and not well fitted by standard active galactic nuclei (AGN) SED templates, without adding extra dust extinction to fit the *WISE* 3.4 and 4.6 μm data. The SCUBA-2 850 μm observations confirm that the Hot DOGs have less cold and/or more warm dust emission than standard AGN templates, and limit an underlying extended spiral or ULIRG-type galaxy to contribute less than about 2 or 55 per cent of the typical total Hot DOG IR luminosity, respectively. The two most distant and luminous targets have similar observed submm to mid-infrared ratios to the rest, and thus appear to have even hotter SEDs. The number of serendipitous submm galaxies detected in the 1.5-arcmin-radius SCUBA-2 850 μm maps indicates there is a significant overdensity of serendipitous sources around Hot DOGs. These submm observations confirm that the *WISE*-selected ultraluminous galaxies have very blue mid-infrared to submm SEDs, suggesting that they contain very powerful AGN, and are apparently located in unusual arcmin-scale overdensities of very luminous dusty galaxies.

Key words: galaxies: active – galaxies: formation – galaxies: high-redshift – infrared: galaxies – submillimetre: galaxies.

1 INTRODUCTION

Ultraluminous infrared galaxies (ULIRGs)¹ were first discovered in the 1980's by the *Infrared Astronomical Satellite* (*IRAS*; Houck et al. 1984; Soifer et al. 1984). More than 90 per cent of their lu-

minosity is emitted in the infrared (IR) due to interstellar dust absorbing ultraviolet (UV) and optical emission produced by active galactic nuclei (AGN) and/or starbursts. The dust then re-emits thermally at longer wavelengths, from the near-IR to millimetre (mm) wavebands.

ULIRGs evolve strongly with redshift, becoming more abundant with a surface density of several hundred per square degree at $z \sim 1$. Out to $z \sim 1$, the evolution rate of luminous dusty galaxies goes as $\sim (1+z)^4$ (Blain et al. 1999; Le Floch et al. 2005). To $z \geq 1$ ULIRGs along with luminous infrared galaxies (LIRGs),¹ account for 70 ± 15 per cent of cosmic star formation activity

*E-mail: sfj8@le.ac.uk

¹LIRGs, ULIRGs and HyLIRGs have characterizing total IR luminosities (8–1000 μm) of $L_{8-1000 \mu\text{m}} > 10^{11} L_{\odot}$, $L_{8-1000 \mu\text{m}} > 10^{12} L_{\odot}$ and $L_{8-1000 \mu\text{m}} > 10^{13} L_{\odot}$.

(Le Floch et al. 2005; Richards et al. 2006). Therefore, at the peak of the cosmic star formation rate (SFR), $z \sim 2-3$, ULIRGs contribute a significant amount to the total IR luminosity density (Smail, Ivison & Blain 1997; Genzel & Cesarsky 2000; Blain et al. 2002; Cowie, Barger & Kneib 2002; Chapman et al. 2005; Le Floch et al. 2005; Hopkins et al. 2008; Reddy et al. 2008; Magnelli et al. 2009, 2012; Elbaz et al. 2011; Casey et al. 2012; Melbourne et al. 2012; Lu et al. 2013). Studying the most extreme IR galaxies at this epoch, should provide a larger and more complete sample of different types of the most luminous AGN, to help in fully understanding the processes of formation and evolution of massive galaxies.

A popular theory for the origin of ULIRGs is that major mergers between massive, gas-rich galaxies provide tidal torques that transport gas to the centre of the more massive galaxy (Barnes & Hernquist 1992; Schweizer 1998; Farrah et al. 2001; Veilleux, Kim & Sanders 2002; Hopkins et al. 2006, 2008). This influx of gas can induce rapid star formation and/or AGN fuelling (Barnes & Hernquist 1992; Mihos 1996; Hopkins et al. 2008): starburst activity dominates the luminosity at first, and then the embedded supermassive black hole (SMBH) grows to dominate. Feedback from the SMBH (radiation, winds and/or jets) and supernovae can expel gas and dust, terminating further star formation and for a short time leaving a visible optical quasar (QSO): finally, a passive massive elliptical galaxy is left behind (Sanders & Mirabel 1996; Hopkins et al. 2006, 2008; Farrah et al. 2012; Spoon et al. 2013). Observations of other dusty galaxy populations could be evidence of different stages of this merging galaxy theory. For example, submillimetre galaxies (SMGs) appear to be high-redshift ULIRGs (Blain et al. 2002; Tacconi et al. 2008) and dust-obscured galaxies (DOGs) have comparable SFRs and IR luminosities to SMGs (Bussmann et al. 2009; Tyler et al. 2009; Melbourne et al. 2012). There could be an evolutionary connection between ULIRGs, SMGs, DOGs, QSOs and massive elliptical galaxies (Sanders et al. 1988a,b).

Luminous, dusty active galaxies heated by AGN and/or recent starburst activity emit in the IR at wavelengths traced by the *Wide-field Infrared Survey Explorer* (WISE) filters at 12 μm (W3) and 22 μm (W4) bands. Eisenhardt et al. (2012), Wu et al. (2012) and Bridge et al. (in preparation.) have shown that WISE can find different classes of interesting, luminous, high-redshift, dusty galaxies. Based on WISE colours and flux cuts, a population has faint or undetectable flux densities in the 3.4 μm (W1) and 4.6 μm (W2) bands, while being well detected (signal-to-noise ratio (SNR) > 5 in the All-Sky WISE Source Catalog²) in the 12 and/or 22 μm bands. These galaxies have been called ‘W1 W2-dropouts’ (Eisenhardt et al. 2012) and Hot DOGs (Wu et al. 2012).

In the major merger theory, the SMG population would represent an earlier, starburst-dominated phase of merging galaxies, and the luminous DOG population are the later, most luminous AGN-dominated phase of merging galaxies, and in energetic terms could easily become optically visible QSOs (Narayanan et al. 2010). The Hot DOGs presented in this paper would qualify the DOG selection criterion, $F_{24\mu\text{m}} > 0.3\text{ mJy}$ and $R - [24] > 14$ (where R is the Vega magnitudes for optical R band and *Spitzer* mid-IR 24 μm ; Dey et al. 2008); however, the Hot DOGs are more luminous, hotter and rarer than typical DOGs and could be extreme cases of DOGs or another stage of merging galaxies (Wu et al. 2012). To investigate this Hot DOG population, follow-up spectroscopy of more than 100 of them revealed that these galaxies are intrinsically very luminous, potentially putting them in the class of ULIRGs¹ and

hyper-luminous infrared galaxies (HyLIRGs¹; Sanders & Mirabel 1996; Lonsdale, Farrah & Smith 2006; Bridge et al., in preparation; Eisenhardt et al., in preparation; Tsai et al., in preparation). They are frequently found in the redshift range $2 < z < 3$ (Eisenhardt et al. 2012; Wu et al. 2012; Bridge et al. 2013), and so far the highest redshift is $z = 4.59$ for W2246–0526 (Tsai et al., in preparation). Their SEDs show a mid-IR to far-IR colour that is too blue to be well fitted by many standard AGN templates, suggesting that they represent a short evolutionary phase of merging galaxies, where an AGN is fuelling very rapidly inside a thick dust shroud, leading to very intense mid-IR but obscured emission and a hot SED, as proposed by Wu et al. (2012), Bridge et al. (2013), Assef et al. (in preparation). The Hot DOGs should show the impact of an AGN on the surrounding interstellar medium at its very greatest. These WISE-selected sources are certainly not typical galaxies, but the processes taking place within them should be at work everywhere.

In this paper, James Clerk Maxwell Telescope (JCMT) Submillimetre Common-User Bolometer Array 2 (SCUBA-2; Holland et al. 2013) observations of 10 Hot DOGs are reported. These long wavelength measurements are needed to understand the cold dust properties and to calculate the total luminosity all the way from 8 to 1000 μm ($L_{8-1000\mu\text{m}}$). Section 2 describes the sample, along with the details of WISE and SCUBA-2 observations. Section 3 reports the SCUBA-2 results, and the SEDs and total IR luminosities ($L_{8-1000\mu\text{m}}$) of the Hot DOGs in comparison with other populations. Existing SED templates of well-studied objects are compared to find out the nature of the Hot DOGs, and their accuracy and a need for additional mid-IR extinction to fit the data is discussed. The submm to mid-IR ratios are discussed, to investigate if the Hot DOG SEDs are dominated by AGN emission or star formation. The luminosities of an underlying extended host galaxy component are calculated, in order to calculate the potential host galaxy contribution to the typical Hot DOG total IR luminosity, to see if the Hot DOGs are dominated by AGN or starburst activity. To see if there is an overdensity of SMGs in the SCUBA-2 fields, SMG number counts are compared to those in other submm surveys.

Throughout this paper, we assume a Λ cold dark matter cosmology with $H_0 = 71\text{ km s}^{-1}\text{ Mpc}^{-1}$, $\Omega_m = 0.27$ and $\Omega_\Lambda = 0.73$ (Hinshaw et al. 2009). WISE catalogue magnitudes are converted to flux densities using zero-point values on the Vega system of 306.7, 170.7, 29.04 and 8.284 Jy for WISE 3.4, 4.6, 12 and 22 μm wavelengths, respectively (Wright et al. 2010).

2 OBSERVATIONS

2.1 WISE

WISE was launched in 2009 December and surveyed the entire sky at wavelengths of 3.4, 4.6, 12 and 22 μm (Wright et al. 2010). One of the primary science goals was to identify the most luminous galaxy in the observable Universe, which can be accomplished due to WISE obtaining much greater sensitivity than previous all-sky IR survey missions. For example, IRAS yielded catalogued source sensitivities of 0.5 Jy at 12, 25 and 60 μm and 1 Jy at 100 μm (Neugebauer et al. 1984). WISE achieved 5σ source sensitivities better than 0.054, 0.071, 0.73 and 5.0 mJy and angular resolutions of 6.1, 6.4, 6.5 and 12.0 arcsec in the W1 to W4 bands, respectively (Wright et al. 2010; Jarrett et al. 2011).

² <http://wise2.ipac.caltech.edu/docs/release/allsky/>

Table 1. Coordinates and photometry of the 10 Hot DOGs, with 3.4, 4.6, 12 and 22 μm magnitudes from the AllWISE Source Catalog and 850 μm flux densities from SCUBA-2. The top six targets are detected at 850 μm , while the bottom four targets have upper limits at 850 μm . The targets with *WISE* upper limits have $\text{SNR} < 2$ and therefore in the AllWISE Source Catalog the magnitudes quoted are 2σ upper limits. For redshifts of the targets refer to Eisenhardt et al. (in preparation) and Bridge et al. (in preparation).

Source	RA (J2000)	Dec. (J2000)	3.4 μm (mag)	4.6 μm (mag)	12 μm (mag)	22 μm (mag)	850 μm (mJy)	850 μm / 22 μm (Ratio)	Redshift
W0831+0140	08:31:53.30	+01:40:10.8	17.92 ± 0.28	16.10 ± 0.20	10.15 ± 0.07	7.28 ± 0.12	9.3 ± 2.1	0.9 ± 0.2	3.91
W1136+4236	11:36:34.31	+42:36:02.6	18.19 ± 0.24	15.83 ± 0.11	10.62 ± 0.07	7.66 ± 0.11	5.3 ± 1.7	0.7 ± 0.1	2.39
W1603+2745	16:03:57.40	+27:45:53.3	< 18.02	17.04 ± 0.34	9.89 ± 0.04	7.28 ± 0.11	10.2 ± 1.8	1.0 ± 0.2	2.63
W1835+4355	18:35:33.73	+43:55:48.7	17.44 ± 0.09	15.20 ± 0.05	9.15 ± 0.03	6.19 ± 0.04	8.0 ± 1.5	0.3 ± 0.1	2.30
W2216+0723	22:16:19.09	+07:23:54.5	17.33 ± 0.16	15.59 ± 0.13	9.91 ± 0.05	6.91 ± 0.09	5.5 ± 1.6	0.4 ± 0.1	1.68
W2246−0526	22:46:07.54	−05:26:35.1	17.54 ± 0.21	16.65 ± 0.37	10.27 ± 0.09	6.80 ± 0.11	11.4 ± 2.1	0.7 ± 0.1	4.59
W1814+3412	18:14:17.31	+34:12:24.8	18.86 ± 0.44	17.61 ± 0.49	10.41 ± 0.06	6.86 ± 0.07	2.0 ± 1.8	< 0.4	2.45
W2026+0716	20:26:15.27	+07:16:23.9	17.58 ± 0.21	15.69 ± 0.13	10.18 ± 0.07	7.31 ± 0.11	2.0 ± 1.7	< 0.6	2.54
W2054+0207	20:54:25.69	+02:07:11.0	18.27 ± 0.32	15.32 ± 0.09	9.59 ± 0.05	7.13 ± 0.09	3.3 ± 1.8	< 1.1	2.52
W2357+0328	23:57:10.82	+03:28:03.4	< 18.14	< 16.61	10.09 ± 0.07	6.94 ± 0.11	2.2 ± 1.9	< 0.4	2.12

2.2 Target selection

The objects observed here are selected from the *WISE* All-Sky Source catalog², with IR magnitudes derived using point source profile-fitting (Cutri et al. 2012). The Hot DOG selection criteria are to have a faint or undetectable flux in *W1* and *W2*, but a detectable flux ($\text{SNR} > 5$) in *W3* and/or *W4*. The selected galaxies have *W1* > 17.4 mag and either *W4* < 7.7 mag and *W2* − *W4* > 8.2 or *W3* < 10.6 mag and *W2* − *W3* > 5.3 (Eisenhardt et al. 2012). The search was made greater than 30° away from the Galactic Centre and 10° from the Galactic plane to avoid enhanced levels of saturation artefacts and stars.

The number of *WISE*-selected Hot DOGs over the extragalactic sky, to this magnitude limit, is about 1000, which points to this population being extremely rare, and perhaps a transitional population (Eisenhardt et al. 2012; Assef et al., in preparation; Tsai et al., in preparation). The JCMT targets were selected because they had known spectroscopic redshifts (Bridge et al., in preparation; Eisenhardt et al., in preparation), could be observed in the A-semester (January–July) at the JCMT, and were queued to obtain *Herschel* data (Bridge et al., in preparation; Tsai et al., in preparation). We selected 31 targets and obtained observations of 10 targets with SCUBA-2 that were chosen at random due to the vagaries of the queue observing system. Their *WISE* *W4* band fluxes were selected to be among the greatest of the suitable sources, in the hope of increasing the chance that their 850 μm flux would be bright enough to be detected or limits would be significant. Therefore, with any conclusions drawn it must be remembered that these Hot DOGs have been selected to be mid-IR bright.

The *WISE* flux densities presented in Table 1 are from the subsequent AllWISE Source Catalog,³ that has improved photometric sensitivity and accuracy, and improved astrometric precision compared to the *WISE* All-Sky Source Catalog.

2.3 JCMT SCUBA-2

Ten Hot DOGs were observed with SCUBA-2 on the 15-m JCMT atop Mauna Kea in Hawaii, primarily in 2012 May but also on other nights throughout the 12A-semester, from 2012 January to July.

SCUBA-2 is a bolometer camera and has eight 32×40 pixel detector arrays each with a field of view of 2.4 arcmin^2 (Holland et al.

2013). SCUBA-2 observes in the atmospheric windows at 450 and 850 μm . The diffraction-limited beams have full-width half maxima (FWHM) of approximately 7.5 and 14.5 arcsec, respectively.

The optical depth at 225 GHz, τ_{225} , during the observations was in the range of JCMT Band 2 conditions: $0.05 < \tau_{225} < 0.08$ (Dempsey et al. 2013). The corresponding opacities for each atmospheric window, 450 and 850 μm , were $0.61 < \tau_{450} < 1.18$ and $0.24 < \tau_{850} < 0.40$. Therefore, we could not use any 450 μm data because the atmospheric opacity was too great.

All observations were taken in the ‘CV DAISY’ mode that produces a 12-arcmin-diameter map, with the deepest coverage in a central 3-arcmin-diameter region (Holland et al. 2013). The target stays near the centre of the arrays and the telescope performs a pseudo-circular pattern with a radius of 250 arcsec at a speed of $155 \text{ arcsec s}^{-1}$. This mode is best for point-like sources and those smaller than 3-arcmin. Each scan was 30 min long and four scans were made per target, totalling an exposure time of 120 min per target. The typical 850 μm noise achieved in these DAISY maps was 1.8 mJy/beam, and the noise increases by ~ 10 per cent out to a radius of 1.5-arcmin (Table 1). We have treated only this uniform central region of the SCUBA2 DAISY maps in this analysis.

Pointing checks were taken throughout the night. The calibration sources observed were Uranus, CRL 2688, CRL 618 and Mars. Calibrations were taken at the start and end of every night in the standard manner (Dempsey et al. 2013), and where consistent with the standard values.

3 RESULTS

3.1 Photometry

The maps were reduced with the STARLINK SubMillimeter User Reduction Facility (*SMURF*) data reduction package with the ‘Blank Field’ configuration suitable for low-SNR point sources (Chapin et al. 2013). *SMURF* performs pre-processing steps to clean the data by modelling each of the contributions to the signal from each bolometer, flat-fields and removes atmospheric emission, and finally regrids to produce a science-quality image. Using the STARLINK Pipeline for Combining and Analyzing Reduced Data (*PICARD*) package the maps were mosaicked with all four observations per target, beam-match filtered with a 15-arcsec FWHM Gaussian and calibrated with the flux conversion factor of $2.34 \text{ Jy pW}^{-1} \text{ arcsec}^{-2}$

³ <http://wise2.ipac.caltech.edu/docs/release/allwise/>

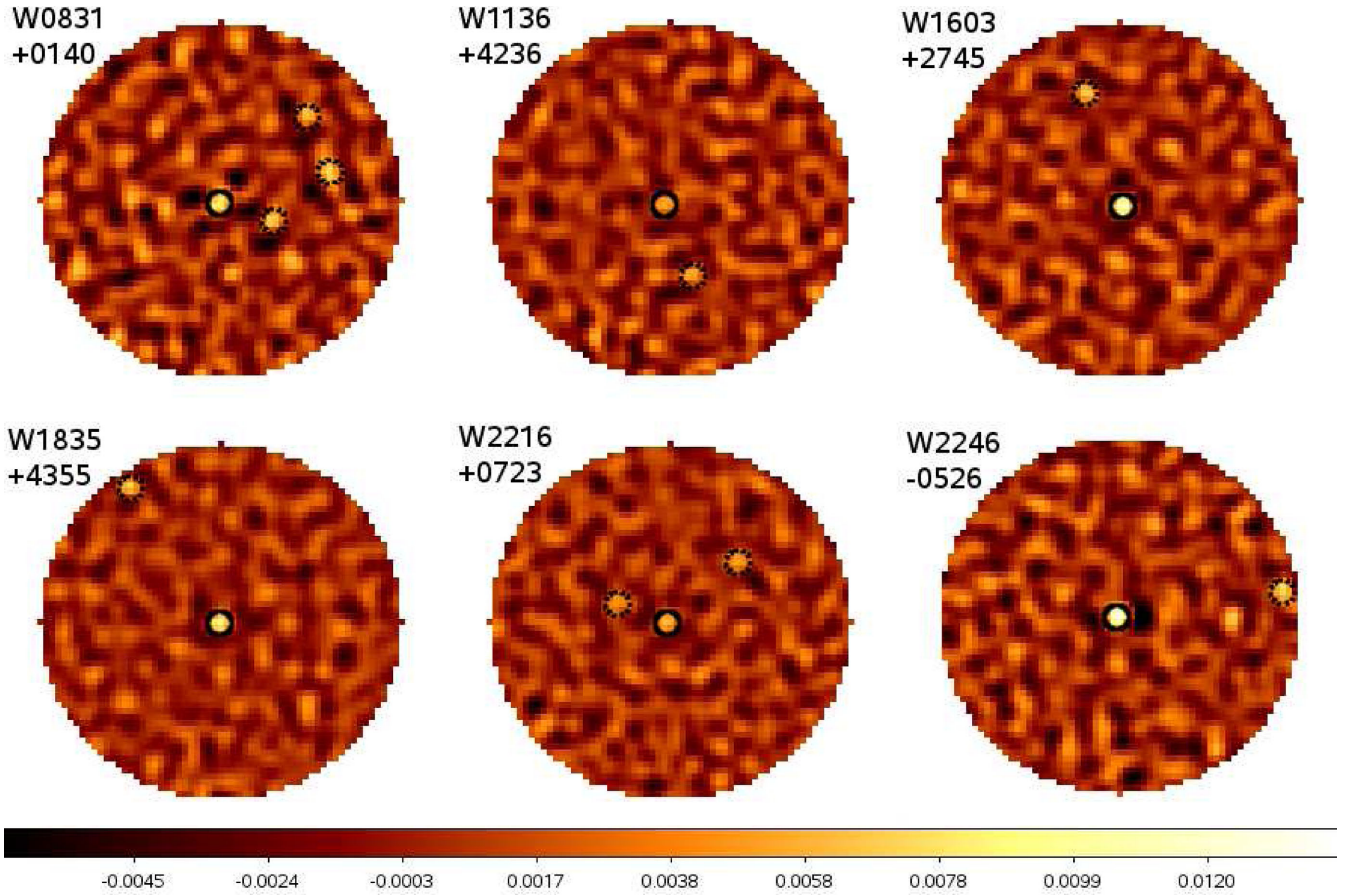


Figure 1. SCUBA-2 850 μm 1.5-arcmin-radius maps of the six detected targets; W0831+0140, W1136+4236, W1603+2745, W1835+4355, W2216+0723 and W2246–0526. The solid circles show the 15-arcmin beam-sized apertures centred on the *WISE* RA Dec. of the targets. Serendipitous sources brighter than 3σ and within 1.5-arcmin-radius of the *WISE* target are shown by the dotted 15-arcmin beam-sized circles. The colour flux bar at the bottom is in Jy. North is up, east is to the left.

(appropriate for aperture photometry) or $537 \text{ Jy pW}^{-1} \text{ beam}^{-1}$ (in order to measure absolute peak fluxes of discrete sources) that is appropriate for 850 μm data (Dempsey et al. 2013).

The 850 μm flux densities of the 10 Hot DOGs at their *WISE* positions and the noise level in the maps are presented in Table 1. Six Hot DOGs are detected at greater than 3σ significance, while the other four targets had positive flux measurements at the *WISE* position with significances between 1.1 and 1.9σ . The flux density limits for all the targets were measured in an aperture diameter of 15 arcsec, which is the same size as the FWHM of the telescope beam. This was an appropriate aperture size: for the detected sources, the aperture flux densities on this scale are consistent with the peak flux densities. Figs 1 and 2 show the sensitive 3-arcmin-diameter SCUBA-2 850 μm DAISY fields of the six detected Hot DOGs and the four undetected Hot DOGs, respectively. The typical error of the *WISE* position compared to the SCUBA-2 position of the detected targets was 1 arcsec.

To test whether the positive flux density of the four targets with upper limits is likely to be real, random points were sampled from the maps, and the stacked average flux density was $0.0 \pm 0.5 \text{ mJy}$. This is consistent with the positive flux densities from the Hot DOGs with upper limits being due to fainter, undetected targets.

W2026+0716 is the only target whose 850 μm flux increases when measured in a larger aperture (see Fig. 3). It has a 850 μm flux density of 2.1 mJy with a 15-arcsec beam-sized aperture. However,

when increasing the diameter to 29 arcsec, the flux density increases to 7.3 mJy. The higher flux is likely because the target has multiple components on scales bigger than the SCUBA-2 beam. Multiple components have been seen in another Hot DOG, W1814+3412, where several objects on scales less than 10 arcsec are apparent (Eisenhardt et al. 2012). Alternatively, there could be an unrelated source or sources. The *WISE* extended source flag is 0 for the W1 through W4 bands, which means that the detected source is not extended at *WISE* wavelengths (see Fig. 3). There are no obvious signs of a cluster of sources nearby in *Spitzer* images (Wu et al. private communication). However, *Herschel* 160 μm imaging shows a possible companion about 10 arcsec away that could contribute enhanced flux in larger apertures in this source (Bridge et al., private communication). Due to this uncertainty, the quoted 850 μm flux density in Table 1 is the 15-arcsec beam-sized aperture flux density (2.1 mJy).

When the images of the four undetected sources are stacked together into one image (Fig. 4) and centred on the *WISE*-determined position of each target, the net flux is $7.8 \pm 2.3 \text{ mJy}$ in the central 15 arcsec region, a net detection of 3.4σ . The four undetected targets are consistent with being on average 2.5 times fainter than the six detected targets. To get deeper observations with SCUBA-2 would require several more hours of integration per target, beyond the existing 120 min, but would not add much more value to this stacked result.

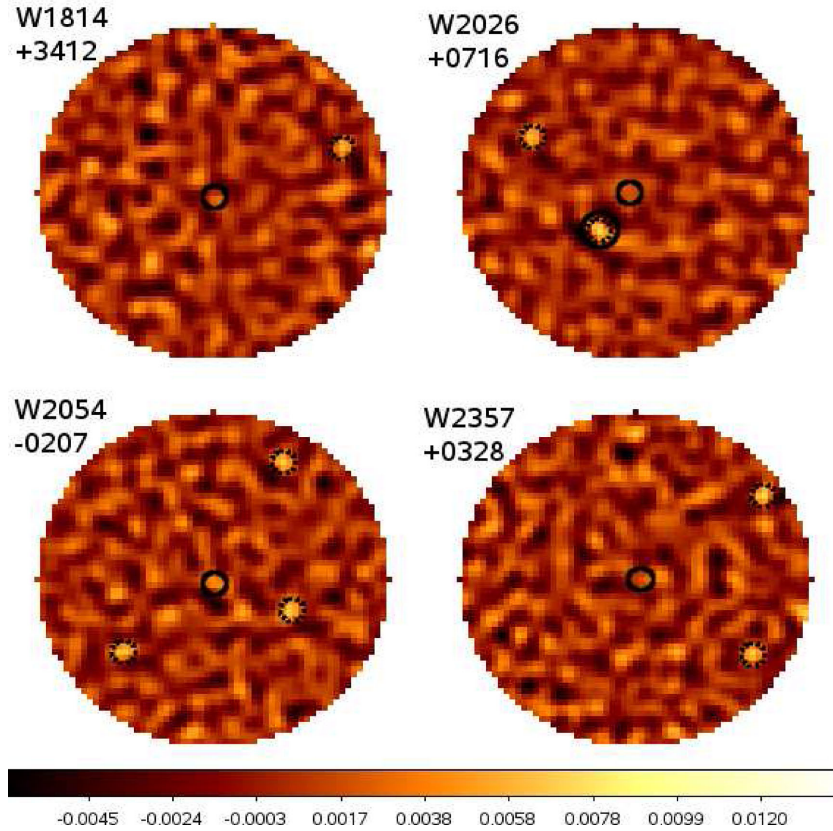


Figure 2. SCUBA-2 850 μm 1.5-arcmin-radius maps of the four undetected targets; W1814+3412, W2026+0716, W2054+0207 and W2357+0328. The solid circles show the 15-arcmin beam-sized apertures centred on the *WISE* RA Dec. of the targets. Serendipitous sources brighter than 3σ and within 1.5-arcmin-radius of the *WISE* target are shown by the dotted 15-arcmin beam-sized circles, and serendipitous source brighter than 4σ is shown by the dotted 15-arcmin beam-sized circle surrounded by a solid black circle. The colour flux bar at the bottom is in Jy. North is up, and east is to the left.

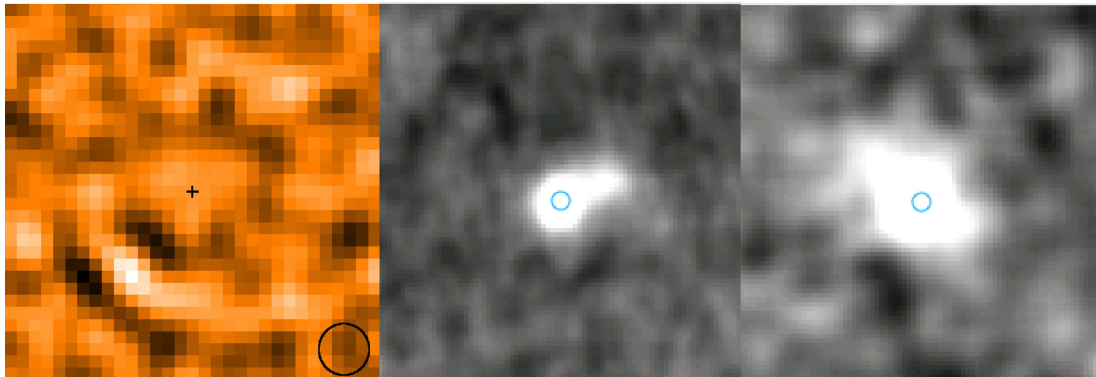


Figure 3. Left: the 2×2 arcmin² SCUBA-2 850 μm map of W2026+0716. Increasing the aperture size out to 29 arcsec in diameter increases the measured flux for this target, which could be due to multiple components of the target or to nearby, unrelated sources. The beam size (15 arcsec diameter) is represented by the black circle. Note the 4.4σ serendipitous source ~ 35 arcsec south-east of the target. Centre and right: *WISE* W3 and W4 images, respectively, showing the same region of sky, with a circle showing the *WISE* determined position of the target. The target is not extended in the *WISE* images. North is up, and east is to the left.

The flux densities presented in Table 1 can be compared with the results of Wu et al. (2012), who observed 14 *WISE*-selected Hot DOGs with the Caltech Submillimeter Observatory (CSO) Submillimeter High Angular Resolution Camera II (SHARC-II) at 350 μm and 18 Hot DOGs with CSO Bolocam at 1.1 mm. Using a 3σ threshold, Wu et al. (2012) found that 9 out of 14 Hot DOGs were detected at 350 μm and 6 of the 18 targets were detected at 1.1 mm. Three sources from the Hot DOG sample in this paper were in

common with Wu et al. (2012); W1603+2745, W1814+3412 and W1835+4355. These CSO results are consistent with our SCUBA-2 observations at 850 μm . The relative sensitivities of SHARC-II and Bolocam are such that we believe the SCUBA-2 detections and limits provide a substantial increase in our knowledge of the HotDOGs' submm properties. Furthermore, W1814+3412 which was detected at 350 μm by Wu et al. (2012), with upper limits reported at 450 and 1100 μm was also detected by the Institut de

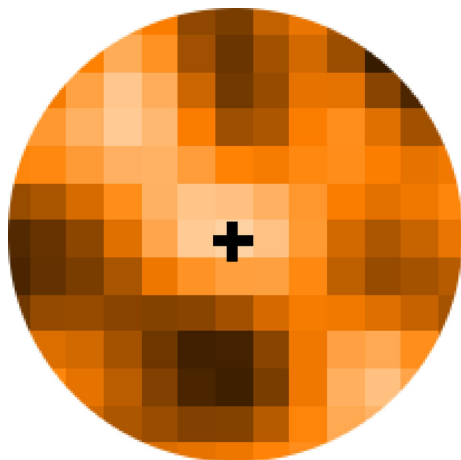


Figure 4. SCUBA-2 850 μm 48 arcsec radius map showing the central region of the four undetected targets stacked together. The cross shows the central pixel. North is up, east is to the left.

Radioastronomie Millimetrique (IRAM) Plateau de Bure interferometer in the 1.3 mm band in 2013 (Blain et al., in preparation).

3.2 SEDs

3.2.1 Short wavelength SEDs

The SEDs of the 10 SCUBA-2 Hot DOGs are shown in Fig. 5. The SEDs are normalized at rest frame 3 μm and shown at rest-

frame wavelengths in order to compare to various galaxy SED templates (Polletta et al. 2007) in order to try and understand the Hot DOGs nature. The Polletta galaxy templates are Arp 220 (starburst-dominated galaxy), Mrk 231 (heavily obscured AGN-starburst composite), QSO 1 and 2 (optically-selected QSOs of type 1 and 2) and torus (type-2 heavily-obscured QSO: an accreting SMBH with a hot accretion disc surrounded by dust and Compton-thick gas in a toroidal structure (Krolik & Begelman 1988)). The Hot DOG SEDs are broadly similar. They have a steep red power-law IR (1–5 μm) section with a potential mid-IR peak from hot dust emission, a mid-IR to submm section that appears to be flatter, i.e. less peaked, than the Polletta AGN templates, turning over to a Rayleigh-Jeans spectrum longwards of 200 μm from the coolest dust emission. The mid-IR to submm section is consistent with being ‘flat-topped’ (in f_ν), as suggested by Wu et al. (2012), and consistent with the 850 μm data presented in this paper, and consistent with *Herschel* results from the most luminous Hot DOGs (Tsai et al., in preparation). However, *Herschel* data of Lyman α blobs (LABs; Bridge et al. 2013) that have similar *WISE* colours to the Hot DOGs in this paper show a far-IR peak in the SED. Further discussion of this point and the presentation of *Herschel* follow-up of *WISE* Hot DOGs will be presented by Bridge et al. (in preparation) and Tsai et al. (in preparation).

A better fitting SED model for these Hot DOGs is also shown in Figs 5 and 6. The W1814+3412 template shown is entirely empirical, and assumes a single-temperature dust spectrum representing the minimum dust temperature present (53 ± 5 K), with an emissivity index of $\beta = 1.5$ at longer wavelengths, smoothly interpolated to a power-law spectrum instead of a Wien law at shorter wavelengths, with an opacity factor imposed at the shortest mid-IR wavelengths,

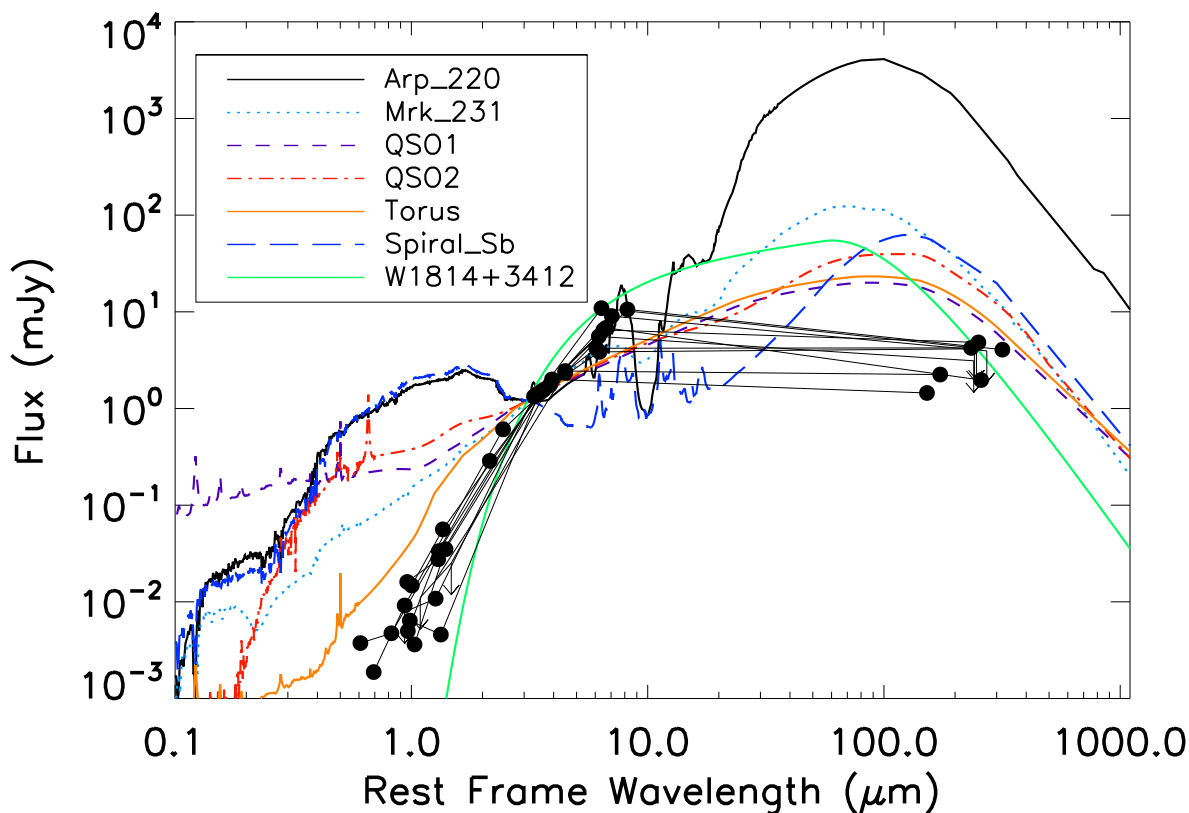


Figure 5. SEDs of the 10 Hot DOGs including the 850 μm SCUBA-2 data in rest-frame wavelengths with Arp 220, Mrk 231, QSO 1, QSO 2 and torus galaxy templates from Polletta et al. (2007) and W1814+3412 template from Blain et al. (in prep.) normalized at 3 μm . Detections are represented by filled circles, while 2σ upper limits are represented by arrows. The data points for the Hot DOGs are connected for clarity, and do not represent the true SED.

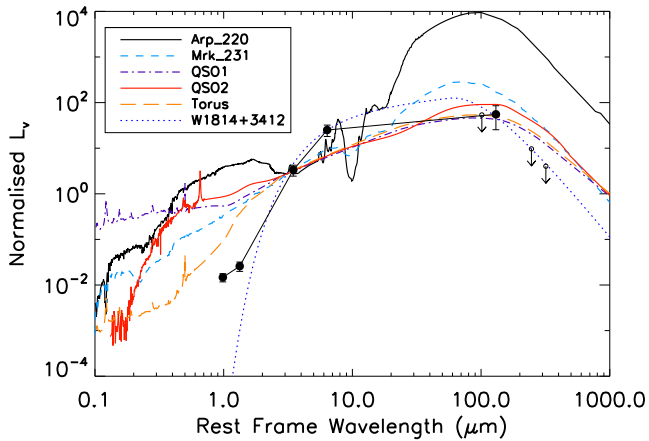


Figure 6. SED of W1814+3412 at $z=2.452$, including the 850 μm SCUBA-2 data with Polletta galaxy templates Arp 220, Mrk 231, QSO 1, QSO 2 and torus (Polletta et al. 2007) and W1814+3412 template (Blain et al. in prep.) normalized at rest-frame 3 μm . CSO SHARC-II 350 μm and 450 μm and CSO Bolocam 1100 μm data points from Wu et al. (2012) are included. Detections are represented by filled circles, while 2σ upper limits are represented by arrows.

to match the *WISE* data, corresponding to a finite total luminosity $L_{8-1000\mu\text{m}} = 4.6 \times 10^{13} L_{\odot}$ for W1814+3412. It is constrained by *Herschel* data from Wu et al. (2012) and IRAM data from Blain et al. (in preparation), and so unsurprisingly provides a better fit than the Polletta et al. (2007) templates that pre-date these observations.

The SEDs are not well fitted by any of the templates; the closest fitting template is the single torus template, although extra dust extinction is required to fit the W1 and W2 data. Between the Polletta torus template and the mean SED of the 850 μm detected targets, both normalized at 3 μm , the extra dust extinction required at rest frame 1 μm is 1.6 mag. Converting to a *V*-band extinction implies an extra dust extinction $A_V \geq 6.8$ mag. Eisenhardt et al. (2012) found significant obscuration in the SED of W1814+3412 with a dust extinction value of $A_V = 48 \pm 4$ in the rest frame from optical SED fitting. The gas column density N_H can be estimated by applying a standard ‘gas-to-extinction’ equation $N_H \approx 2A_V \times 10^{22} \text{ mag}^{-1} \text{ cm}^{-2}$ from Maiolino et al. (2001), which estimates that the extra N_H needed is 10^{23} cm^{-2} . The Polletta torus template was modelled on a heavily obscured type-2 QSO, with a rest-frame N_H of $2.14^{+0.54}_{-1.34} \times 10^{24} \text{ cm}^{-2}$ (Polletta et al. 2006). The extra N_H can be added to the Polletta torus template N_H to estimate the total N_H of the Hot DOGs to be $\sim 2.3 \times 10^{24} \text{ cm}^{-2}$, implying a Compton-thick AGN (Osterbrock & Shaw 1988; Madau, Ghisellini & Fabian 1994; Comastri et al. 1995; Maiolino & Rieke 1995; Risaliti, Maiolino & Salvati 1999; Piconcelli et al. 2003; Treister & Urry 2005). This is consistent with Stern et al. (2014), who observed three Hot DOGs, including W1814+3412 in common with this paper, with *NuSTAR* and *XMM-Newton*, and found that the three targets have gas column densities $N_H \geq 10^{24} \text{ cm}^{-2}$, which implies the targets are Compton-thick AGNs.

3.2.2 Long wavelength SEDs

Normalized to the *WISE* data at rest frame 3 μm that lies within the *WISE* rest-frame wavelength range for all of our Hot DOGs, the SCUBA-2 data show that the Hot DOGs have less submm emission than the Polletta torus template, with an average flux difference factor of 5 between the data and template, and a range of 2–8 factor,

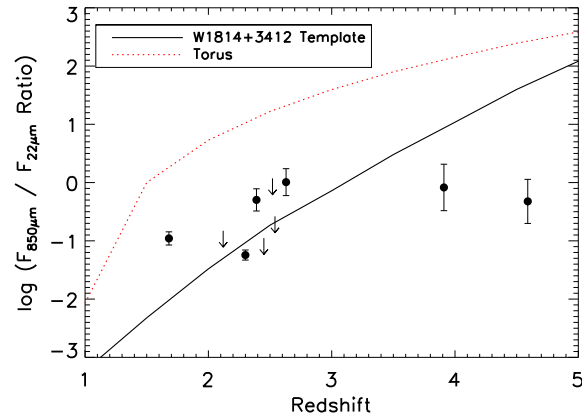


Figure 7. The submm to mid-IR ratio ($F_{850\mu\text{m}}/F_{22\mu\text{m}}$) of the 10 Hot DOGs. The solid line shows the W1814+3412 template (Blain et al., in preparation) and the dotted line shows Polletta torus template (Polletta et al. 2007) as a function of redshift. Detections are represented by filled circles, while 2σ upper limits are represented by arrows.

for the detected targets, and an average flux difference factor of 7 between the data and template, and a range of 6–8, for the undetected targets (limits plus 2σ).

The submm to mid-IR ratio ($F_{850\mu\text{m}}/F_{22\mu\text{m}}$) of the 10 targets in the observed frame are listed in Table 1. The weighted average $F_{850\mu\text{m}}/F_{22\mu\text{m}}$ of the six detected targets is 0.6 ± 0.1 , where the error is the weighted standard error. Fig. 7 shows these ratios in the observed sample, and for the W1814+3412 and Polletta AGN torus templates, as a function of redshift. The subsequent empirical W1814+3412 template provides a better fit to the targets, as expected. Most of the Hot DOGs appear to lie near the W1814+3412 template but show no clear sign of the expected *K*-correction with redshift of the templates: in particular the two highest redshift Hot DOGs (W0831+0140 and W2246–0526) lie beneath both templates with relatively faint submm fluxes, and similar observed submm to mid-IR ratios of the other lower redshift Hot DOGs. They are also the most luminous targets, with IR luminosities, $L_{8-1000\mu\text{m}} > 10^{14} L_{\odot}$ (see Section 3.3), which suggests that they have hotter effective dust temperatures compared with the rest of the sample. Another distant Hot DOG, W0410–0913 at $z = 3.592$, was reported by Wu et al. (2012). It has a submm to mid-IR ratio of 3.2 ± 0.8 ($\log(0.5 \pm 0.1)$), and lies close to the W1814+3412 template.

The Hot DOGs are all consistent with high dust temperatures inferred from the submm/*WISE* data (Wu et al. 2012). The W1814+3412 template (Fig. 6) has a temperature of 53 ± 5 K for the coolest contribution to the SED. Estimates of the temperatures for Hot DOGs and *WISE*-selected LABs have included 60–120 K (Wu et al. 2012) and 40–90 K (Bridge et al. 2013). This is greater than other SMGs and DOGs, which have typical temperatures of 25–40 K (Chapman et al. 2005; Coppin et al. 2008; Magnelli et al. 2012; Melbourne et al. 2012). The definitions of SED shape and temperature contributions can be complex, but the rest-frame peak of the Hot DOG SEDs occurs bluewards of other galaxy classes.

3.3 Luminosities

Total IR luminosities are calculated for each target using a minimal power-law interpolation between the *WISE* and SCUBA-2 data points, and also by using the W1814+3412 template with each targets’ *WISE* and SCUBA-2 data.

Table 2. The total IR luminosities ($8\ \mu\text{m} - \text{SCUBA2}$) of the 10 Hot DOGs derived by connecting all the *WISE* and SCUBA-2 data points with power laws and then integrating. The top six have detections at $850\ \mu\text{m}$ and the bottom four have 2σ upper limits at $850\ \mu\text{m}$. The luminosities are shown in solar luminosities, $3.84 \times 10^{26}\ \text{W}$. The W1814+3412 template total IR luminosities $L_{8-1000\ \mu\text{m}}$ are found by using the Blain et al. (in preparation) W1814+3412 template with the Hot DOGs' SCUBA-2 data. The total IR luminosities ($8-1000\ \mu\text{m}$) of two targets also observed by Wu et al. (2012) are $4.0 \times 10^{13}\ L_{\odot}$ for W1814+3412, and $6.5 \times 10^{13}\ L_{\odot}$ for W1835+4355, are consistent with the luminosities in the table below.

Source	Total IR luminosities ($8\ \mu\text{m} - \text{SCUBA2}$) (L_{\odot})	W1814+3412 template Total IR luminosities ($8-1000\ \mu\text{m}$) (L_{\odot})
W0831+0140	$8.7 \pm 1.8 \times 10^{13}$	$3.6 \pm 1.6 \times 10^{14}$
W1136+4236	$1.5 \pm 4.6 \times 10^{13}$	$6.2 \pm 3.8 \times 10^{13}$
W1603+2745	$3.1 \pm 0.7 \times 10^{13}$	$1.5 \pm 0.5 \times 10^{14}$
W1835+4355	$4.3 \pm 4.1 \times 10^{13}$	$8.5 \pm 3.4 \times 10^{13}$
W2216+0723	$1.0 \pm 1.8 \times 10^{13}$	$2.7 \pm 1.6 \times 10^{13}$
W2246-0526	$1.3 \pm 2.9 \times 10^{14}$	$6.4 \pm 2.4 \times 10^{14}$
W1814+3412	$< 2.5 \times 10^{13}$	$< 7.0 \times 10^{13}$
W2026+0716	$< 2.1 \times 10^{13}$	$< 7.3 \times 10^{13}$
W2054+0207	$< 2.9 \times 10^{13}$	$< 9.2 \times 10^{13}$
W2357+0328	$< 1.9 \times 10^{13}$	$< 5.3 \times 10^{13}$

A conservative lower limit to the total IR luminosities of the galaxies were estimated by connecting all the *WISE* and SCUBA-2 data points with power laws and then integrating, without extrapolating beyond the range of the data in wavelength. This luminosity is a conservative estimate because any strong peak in the SED would not be included on the power-law interpolation. The resulting $L_{8\ \mu\text{m}-\text{SCUBA2}}$ values for the 10 Hot DOGs are presented in Table 2. The six detected targets have values that range from $(1.0 \pm 1.8) \times 10^{13}\ L_{\odot}$ to $(1.3 \pm 2.9) \times 10^{14}\ L_{\odot}$, with one having $L_{8\ \mu\text{m}-\text{SCUBA2}} \geq 10^{14}\ L_{\odot}$. This classifies them all as HyLIRGs.

The $L_{8-1000\ \mu\text{m}}$ are also found by fitting the W1814+3412 template from Blain et al. (in preparation) with the targets' SCUBA-2 data. The W1814+3412 template was used because it is based on data from *WISE*, *Herschel* and IRAM of the Hot DOG W1814+3412 that are near the peak of the SED. The six detected targets assuming the W1814+3412 template, yield luminosities from $(2.7 \pm 1.6) \times 10^{13}\ L_{\odot}$ to $(6.4 \pm 2.4) \times 10^{14}\ L_{\odot}$, the factor of ~ 4 difference between the two methods for calculating the luminosities is due to the systematic uncertainties of the SED.

Our total IR luminosity of W1835+4355 ($L_{8\ \mu\text{m}-\text{SCUBA2}} = 4.0 \pm 4.1 \times 10^{13}\ L_{\odot}$), the source also observed by CSO, is consistent with $L_{8-1000\ \mu\text{m}} = 6.5 \times 10^{13}\ L_{\odot}$ reported in Wu et al. (2012). The derived luminosity of the W1814+3412 template from Blain et al. (in preparation) was $L_{8-1000\ \mu\text{m}} = 4.6 \times 10^{13}\ L_{\odot}$ and compared with the luminosity calculated using the *WISE* and SCUBA-2 data was $L_{8\ \mu\text{m}-\text{SCUBA2}} < 2.0 \times 10^{13}\ L_{\odot}$, is slightly higher due to the W1814+3412 template included CSO SHARC-II data, which is nearer the peak of the SED.

Exceptionally bright galaxies can often be found to be gravitational lensed, for example Eisenhardt et al. (1996); Williams & Lewis (1996); Solomon & Vanden Bout (2005); Vieira et al. (2010); Negrello et al. (2010); Bussmann et al. (2013). However, the Hot DOG luminosities are thought to be intrinsic and not due to gravitational lensing: high-resolution imaging programmes (Bridge et al., in preparation; Petty et al., in preparation) from *Hubble Space Telescope* (*HST*) and ground-based telescopes of a subset of Hot DOGs show no obvious lensed structures (Wu et al. 2014). Resolved near-

IR *HST* observations show the population to have a range of morphologies from clumpy and extended to point-like (Bridge et al., in preparation; Petty et al., in preparation). This suggests that the Hot DOGs are indeed amongst the most intrinsically luminous galaxies in the Universe (Eisenhardt et al. 2012; Tsai et al., in preparation).

The four undetected Hot DOGs each have $L_{8\ \mu\text{m}-\text{SCUBA2}} \leq 10^{13}\ L_{\odot}$ (Table 2). The stacked $850\ \mu\text{m}$ flux density ($7.8 \pm 2.3\ \text{mJy}$) of the four targets with $850\ \mu\text{m}$ upper limits was used with the W1814+3412 template to estimate the luminosity $L_{8-1000\ \mu\text{m}} = (9.3 \pm 4.7) \times 10^{13}\ L_{\odot}$, which is consistent with a HyLIRG. A higher luminosity could be found if there are *Herschel* detections of a significant peak in the far-IR (Bridge et al., in preparation; Tsai et al., in preparation).

We also use the SCUBA-2 data to limit the luminosity of an underlying extended galaxy. A spiral (Sb) galaxy template and a warmer ULIRG-type (Arp 220) template were fitted to account for all of the SCUBA-2 $850\ \mu\text{m}$ flux density, and then by integrating under the Sb or Arp 220 template, the maximum total luminosity of this template SED can be estimated. This approach assumes that an underlying extended dusty galaxy, disconnected from the mid-IR emission, accounts for all of the measured SCUBA-2 flux. This extended emission can be assumed to all be due to star-formation rather than an AGN. An Sb host galaxy template cannot exceed ~ 2 per cent of the inferred Hot DOG luminosity from $8-1000\ \mu\text{m}$. This would give a Sb luminosity of $1.3 \times 10^{12}\ L_{\odot}$; 22 times more luminous than the Milky Way ($6 \times 10^{10}\ L_{\odot}$), with an equivalent SFR of $\sim 30\ M_{\odot}\ \text{yr}^{-1}$, which is lower than the UV-derived SFR of $\sim 300\ M_{\odot}\ \text{yr}^{-1}$ derived for W1814+3412 (Eisenhardt et al. 2012). An Arp 220 ULIRG template can account for the $850\ \mu\text{m}$ data, if the host galaxy has a luminosity of $2.9 \times 10^{13}\ L_{\odot}$, ~ 55 per cent of the inferred Hot DOG luminosity, with an equivalent SFR of $\sim 450\ M_{\odot}\ \text{yr}^{-1}$. This emphasizes that the full Hot DOG SED from $8-1000\ \mu\text{m}$ has a small contribution from cold far-IR dust and is dominated by hot dust and mid-IR emission.

3.4 Clustering

There is significant evidence from previous studies that the galaxy density in the environments of high-redshift far-IR and mid-IR luminous galaxies and SMGs appears to be above average (Scott et al. 2002; Blain et al. 2004; Borys et al. 2004; Farrah et al. 2006; Scott, Dunlop & Serjeant 2006; Gilli, Comastri & Hasinger 2007; Chapman et al. 2009; Cooray et al. 2010; Hickox et al. 2012). Clustering of SMGs could be evidence of massive dark matter haloes associated with the SMGs at high redshift. To investigate if there is clustering of SMGs in the Hot DOG fields, the serendipitous sources number counts will be compared with the number counts from two different blank-field submm surveys. To provide another way to test SMG clustering in the Hot DOG fields, 1.5-arcmin-radius circles will be placed at random and centred on SMG detections in a blank-field submm survey.

17 serendipitous $850\ \mu\text{m}$ sources were detected at greater than 3σ in the 10 SCUBA-2 maps, and one source was detected at greater than 4σ ; see Table 3. The total area surveyed is $71\ \text{arcmin}^2$, or about 1500 SCUBA-2 $850\ \mu\text{m}$ beams. Figs 1 and 2 show the location of detected serendipitous sources in the SCUBA-2 fields of all the detected and undetected Hot DOGs, respectively. There are 4 ± 2 negative peaks in the 10 maps at above the same 3σ threshold (see Table 3), consistent with the $2 \pm 1\ 3\sigma$ negative peaks expected from Gaussian noise.

To see if there is evidence for an overdensity of SMGs in the 10 SCUBA-2 Hot DOG fields, the number of serendipitous sources

Table 3. Number of serendipitous sources in each of the 10 maps at greater than 3σ and 4σ significance, and the number of negative peaks at greater than 3σ significance. There were no negative peaks at greater than 4σ in the 10 maps.

Source	Number of serendipitous sources at greater than 3σ	Number of serendipitous sources at greater than 4σ	Number of negative peaks at greater than 3σ
W0831+0140	3	0	0
W1136+4236	1	0	0
W1603+2745	1	0	0
W1814+3412	1	0	1
W1835+4355	1	0	0
W2026+0716	2	1	1
W2054+0207	3	0	1
W2216+0723	2	0	0
W2246−0526	1	0	1
W2357+0328	2	0	0

can be compared with the results of field submm surveys. In the LABOCA ECDFS Submillimeter Survey (LESS), Weiß et al. (2009) detected 126 SMGs in a uniform area of 1260 arcmin^2 with a noise level of 1.2 mJy at $870 \mu\text{m}$. They also found evidence for an angular two-point clustering signal on angular scales smaller than 1 arcmin . There are 101 LESS sources brighter than our average 3σ flux density limit of 5.3 mJy , which implies 5.7 serendipitous sources would be expected in our 10 SCUBA-2 fields; however, we find 15. This indicates a relative overdensity of SMGs in our Hot DOG fields by a factor of 2.6 ± 0.7 . The noise level range of our maps is $1.5\text{--}2.1 \text{ mJy beam}^{-1}$. In order to check the effect of our range of sensitivity in each field, we also compare the number of SMGs at our highest noise level ($2.1 \text{ mJy beam}^{-1}$) with to the LESS survey. The number of LESS sources brighter than our greatest 3σ flux density limit of 6.3 mJy is 60 SMGs, which implies that 3.4 serendipitous sources would be expected in our 10 SCUBA-2 fields. However, we find nine and thus a relative overdensity of SMGs by a factor of 2.7 ± 1.0 . The overdensity using the highest noise level is consistent with that using the average noise level; therefore, the difference in the 10 map noise levels appears not to have a large effect on the overdensity factor.

A complementary way to test whether there is an overdensity of SMGs near the Hot DOG targets is to place 1.5-arcmin -radius circles at random locations in the LESS field and count the number of sources from the catalogue source positions that would have been detected in our survey, taking into account the differences in depth, by employing a flux density limit of 5.3 mJy . The 1.5-arcmin -radius circles were chosen because the SCUBA-2 maps were 1.5-arcmin in radius. In 10 sets of 10 randomly selected 1.5-arcmin -radius circles within LESS, we found 7 ± 3 LESS sources brighter than 5.3 mJy , to mimic our SCUBA-2 images in this surveyed field. The total number of 1.5-arcmin -radius fields available within LESS is ~ 200 . There is thus a hint of evidence for a relative overdensity of SMGs around Hot DOGs by a factor of 2.1 ± 1.0 as compared with this blank-field.

A third way to test the overdensity of SMGs in the SCUBA-2 fields is to compare the number of LESS sources brighter than 5.3 mJy within 1.5-arcmin -radius circles centred on LESS-detected sources. In 101 available positions, there are 18 not counting the LESS sources on which each 1.5-arcmin -radius field was centred. This suggests that in 10 SCUBA-2 fields centred on LESS detections there would be only 1.8 serendipitous sources detected; however, we find 15 centred on *WISE*-selected targets, potentially giving a Hot DOG to SMG companion overdensity factor of order 8.

We can repeat this approach in another submm blank-field survey. Casey et al. (2013) used SCUBA-2 to observe the Cosmic Evolution Survey (COSMOS) field over a uniform area of 394 arcmin^2 at a noise level of 0.80 mJy at $850 \mu\text{m}$ and detected 99 SMGs brighter than 3.6σ . There are 18 COSMOS sources brighter than our average detection threshold of 5.3 mJy (3σ), which would imply 6.3 serendipitous sources expected in the 10 SCUBA-2 Hot DOG fields. We find 15, implying a relative overdensity of SMGs by a factor of 2.4 ± 0.7 , which is consistent with 2.6 ± 0.7 from LESS. The number of sources brighter than our greatest 3σ flux density limit of 6.3 mJy is 18 SMGs, which implies that 3.2 serendipitous sources would be expected in our 10 SCUBA-2 fields. However, we find nine and thus a relative overdensity of SMGs by a factor of 2.8 ± 1.1 , which is consistent with 2.7 ± 1.0 from LESS. Again, the variation in noise levels of the 10 Hot DOG field does not appear to have a large effect on the overdensity factor. These results are consistent with the LESS survey. Random 1.5-arcmin -radius circles were not placed in the COSMOS field due to the small size of the field, with only ~ 50 1.5-arcmin -radius fields available.

The six detected Hot DOG targets and the four undetected Hot DOG targets have similar numbers of serendipitous sources, see Figs 1 and 2. The overdensity of SMGs around detected and undetected Hot DOGs appear to be comparable.

Fig. 8 shows the fraction of the total number of serendipitous sources for the 10 SCUBA-2 maps found within $0.25, 0.5, 0.75, 1.0, 1.25$ and 1.5-arcmin from the *WISE* target. The expected fraction of the total number of serendipitous sources with no angular clustering is also plotted on Fig. 8. There is no hint of angular clustering of serendipitous sources around the Hot DOGs on these scales, despite the greater average density of submm sources in the *WISE* fields as compared with blank-field surveys. Clustering of SMGs on larger scales could be expected because there is tentative evidence of clustering from previous submm studies on scales up to $\sim 8 \text{ arcmin}$ (Scoville et al. 2000; Blain et al. 2004; Greve et al. 2004; Farrah et al. 2006; Ivison et al. 2007; Weiß et al. 2009; Cooray et al. 2010; Scott et al. 2010; Hickox et al. 2012). Nevertheless, the lack of a clear two-point correlation signal is interesting, because SMG clustering observations can constrain of the nature of the host haloes around SMGs (Cooray et al. 2010).

4 DISCUSSION

The above results obtained for the Hot DOGs will be discussed by comparing their SEDs and luminosities with other galaxy

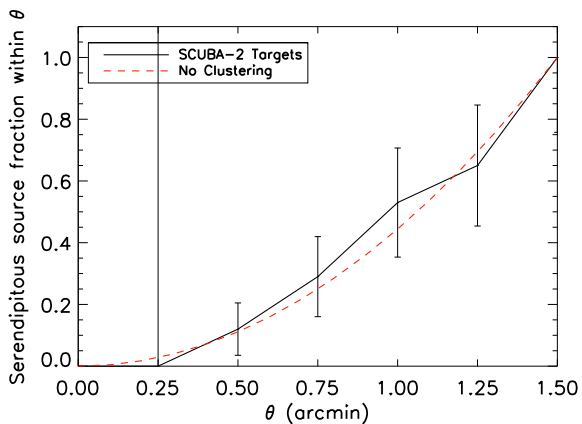


Figure 8. The fraction of the total number of serendipitous sources in each field within different radii of the *WISE* targets. The solid line shows the fields of the Hot DOGs. The dash-dotted line shows the expected number of serendipitous sources if they are randomly located with no clustering. The beam size of SCUBA-2 at $850\ \mu\text{m}$ is $14.5\ \text{arcsec}$; serendipitous sources cannot be detected within the beam.

populations. Next, the Hot DOGs environments are investigated by comparing the serendipitous source number counts to other submm surveys.

The Hot DOG SEDs in Fig. 5 show a blue mid-IR to submm colour. A Compton-thick AGN torus template would fit the Hot DOG SEDs if extra mid-IR extinction of $A_V \geq 6.8\ \text{mag}$ is included. These results can be compared with the SEDs of ULIRGs and LIRGs which have large amounts of obscuring material around the AGN and/or starburst activity, and have estimated dust extinctions between $A_V \simeq 5$ and $50\ \text{mag}$ (Genzel et al. 1998). Comparing the SED of Arp 220 (a starburst-dominated ULIRG) with the Hot DOG SEDs in Fig. 5, reveals that the Hot DOGs appear to have more mid-IR dust extinction than the exceptionally mid-IR red Arp 220. This leads to the conclusion that the Hot DOGs have extremely large amounts of absorption in the AGN torus, and/or host galaxy (Goulding et al. 2012), and could have even larger amounts of obscuring material than typical ULIRGs and LIRGs.

The SCUBA-2 observations show that the Hot DOGs have relatively less submm emission than other galaxy SED templates: the detected Hot DOG targets' SCUBA-2 flux density is on average five times fainter than the Polletta torus template. This leads to the suggestion that the Hot DOGs have less cold dust in the host galaxy and/or on the outer edge of the torus, and hence the torus could be denser, smaller and hotter than in the template. Alternatively, less submm emission could be due to an excess of mid-IR emission from the AGN as compared with the torus template (Wu et al. 2012). The median $850\ \mu\text{m}$ flux density of SMGs, $5.7 \pm 3.0\ \text{mJy}$ (Chapman et al. 2005), is comparable with these Hot DOGs with a median $850\ \mu\text{m}$ flux density of $5.4 \pm 1.8\ \text{mJy}$. Since SMGs and Hot DOGs have similar redshifts ($z \sim 2$), this might suggest comparable cold dust properties. However, to address the degree of similarity between SMGs and Hot DOGs in the far-IR will require knowledge of the far-IR colours of Hot DOGs with data from *Herschel* (Bridge et al., in preparation; Tsai et al., in preparation).

The luminosities of all six detected targets (with a mean luminosity of $L_{8\ \mu\text{m}-\text{SCUBA2}} = 5.3 \times 10^{13}\ L_\odot$ and a median luminosity of $L_{8\ \mu\text{m}-\text{SCUBA2}} = 3.6 \times 10^{13}\ L_\odot$) are greater than those of typical SMGs, which have $L_{8-1000\ \mu\text{m}} = 8.5 \times 10^{12}\ L_\odot$ (Chapman et al. 2005; Kovács et al. 2006), and DOGs, which have a mean luminosity $L_{8-1000\ \mu\text{m}} = 9 \times 10^{12}\ L_\odot$ (Melbourne et al. 2012). This

is in agreement with Wu et al. (2012), who found a sample mean $L_{8-1000\ \mu\text{m}} = 6.1 \times 10^{13}\ L_\odot$ for Hot DOGs. However, the targets in this paper and Wu et al. (2012) could be biased towards being the mid-IR brightest and rarest galaxies, because they were selected on the grounds of their bright mid-IR flux. It is certainly inevitable that deeper mid-IR samples will include DOGs and SMGs; however, our current observed sample of 10, which has a range of *W4* fluxes ($6.19-7.66\ \text{mag}$, or $7.2-27.7\ \text{mJy}$), due to the various selection cuts involved, certainly shows no SMG/ULIRG type SEDs. Eight *WISE*-selected LABs (Bridge et al. 2013) were also found to be ultraluminous galaxies from *Herschel* data ($L_{8-1000\ \mu\text{m}} = 2.3 \times 10^{13}\ L_\odot$), and included a wider range of mid-IR fluxes with no colour cut, again indicating very luminous mid-IR properties of galaxies with extremely red *WISE* colours.

Comparing number counts of the serendipitous sources in the 10 Hot DOG fields with other submm surveys, implies there is an overdensity of SMGs in the 10 SCUBA-2 fields by factor of $\sim 2-3$. This is consistent with finding Hot DOGs in potentially overdense environments. Umehata et al. (2014) observed the protocluster SSA22 field with the Astronomical Thermal Emission Camera on the Atacama Submillimeter Telescope Experiment, at $1.1\ \text{mm}$ to a depth of $0.7-1.3\ \text{mJy beam}^{-1}$, and found 10 SMGs are correlated with $z = 3.1$ Lyman α emitters in the protocluster, which suggests that SMGs are formed in dense environments. Our SMG overdensity around Hot DOGs could indicate that Hot DOGs signpost protocluster regions.

These Hot DOGs appear to be very powerful AGN that have more mid-IR emission and mid-IR opacity than AGN in standard galaxy templates. Therefore, the Hot DOGs might be experiencing the most powerful feedback possible and could be an AGN-dominated short evolutionary phase of merging galaxies, and appear to reside in intriguing arcmin-scale overdensities of very luminous, dusty sources.

5 SUMMARY

The results from SCUBA-2 $850\ \mu\text{m}$ observations of 10 *WISE*-selected, high-redshift, luminous, dusty Hot DOGs are as follows.

- (i) The 10 Hot DOGs have SEDs that are not well fitted by the current AGN templates (see Fig. 5). The best-fitting single Polletta torus template (Polletta et al. 2007) needs extra dust extinction to fit the Hot DOG SEDs with extra $A_V \geq 6.8\ \text{mag}$, which could be due to more screening from the host galaxy and/or AGN torus. The N_H was estimated to be $\sim 2.3 \times 10^{24}\ \text{cm}^{-2}$, which is Compton-thick.
- (ii) The Hot DOGs have a lower ratio of cold to hot dust than the Polletta torus template, which could be because there is less cold dust in the host galaxy, and/or the outer AGN torus in the Hot DOGs are smaller. Alternatively there could be more intense mid-IR emission from the inner regions (Wu et al. 2012). *Herschel* observations near the peak of the SED should soon provide more information.
- (iii) Despite being observed over a wide redshift range, the Hot DOGs show uniform submm to mid-IR ratios. The highest redshift, most luminous targets, could thus have hotter dust temperatures than assumed in the templates. However, the number of targets involved is currently only modest and the selection of the targets is sensitive to redshift, owing to very red intense *WISE* colours.
- (iv) The six SCUBA-2 detected Hot DOGs have very high IR luminosities, $L_{8\ \mu\text{m}-\text{SCUBA2}} \geq 10^{13}\ L_\odot$: they are HyLIRGs. These are conservative values as any pronounced peak of the SED would increase these further and could be missed without *Herschel* data. The stacked IR luminosity, $L_{8-1000\ \mu\text{m}} = (9.3 \pm 4.7) \times 10^{13}\ L_\odot$, of

the four undetected targets is consistent with being a HyLIRG. With no obvious signatures of gravitational lensing known, Hot DOGs are amongst the most luminous galaxies.

(v) The luminosity of an underlying extended star-forming galaxy cannot exceed a luminosity ~ 2 per cent (for a cool spiral galaxy template) or ~ 55 per cent (for a warmer ULIRG-like galaxy template) as compared with the typical Hot DOG luminosity, respectively. Our SCUBA-2 observations confirm that Hot DOGs are a mid-IR dominated population.

(vi) When comparing the submm galaxy counts of the 10 1.5-arcmin-radius SCUBA-2 maps observed here to blank-field surveys, there is an overdensity of SMGs on this scale by a factor 3, but no evidence for any angular clustering within these fields.

(vii) The next step to understand these Hot DOGs is with more *Herschel* observations to accurately define the peak of the SED and increase the sample size, presented in future papers (Bridge et al., in preparation; Tsai et al., in preparation). Another subpopulation of galaxies selected with similar *WISE* colours but also selected to be radio bright, that could be AGN quenching star formation by radio jet feedback at the highest rate of AGN fuelling. A larger number of these targets have been observed with SCUBA-2 and Atacama Large Millimeter/submillimeter Array (ALMA), and will be presented in future papers (Jones et al., in preparation; Lonsdale et al., in preparation). These SCUBA-2 observations provide a comparable density analysis.

ACKNOWLEDGEMENTS

The authors would like to thank the anonymous referee for his/her comments and suggestions, which have greatly improved this paper.

SFJ gratefully acknowledges support from the University of Leicester Physics & Astronomy Department. RJA was supported by Gemini-CONICYT grant number 32120009. This publication makes use of data products from the *WISE*, which is a joint project of the University of California, Los Angeles, and the Jet Propulsion Laboratory/California Institute of Technology, funded by the National Aeronautics and Space Administration.

The James Clerk Maxwell Telescope is operated by the Joint Astronomy Centre on behalf of the Science and Technology Facilities Council of the United Kingdom, the Netherlands Organization for Scientific Research, and the National Research Council of Canada. Additional funds for the construction of SCUBA-2 were provided by the Canada Foundation for Innovation. The project ID under which the data were obtained was M12AU010.

REFERENCES

Barnes J. E., Hernquist L., 1992, *ARA&A*, 30, 705
 Blain A. W., Smail I., Ivison R. J., Kneib J.-P., 1999, *MNRAS*, 302, 632
 Blain A. W., Smail I., Ivison R. J., Kneib J.-P., Frayer D. T., 2002, *Phys. Rep.*, 369, 111
 Blain A. W., Chapman S. C., Smail I., Ivison R., 2004, *ApJ*, 611, 725
 Borys C., Scott D., Chapman S., Halpern M., Nandra K., Pope A., 2004, *MNRAS*, 355, 485
 Bridge C. R. et al., 2013, *ApJ*, 769, 91
 Bussmann R. S. et al., 2009, *ApJ*, 705, 184
 Bussmann R. S. et al., 2013, *ApJ*, 779, 25
 Casey C. M. et al., 2012, *ApJ*, 761, 140
 Casey C. M. et al., 2013, *MNRAS*, 436, 1919
 Chapin E. L., Berry D. S., Gibb A. G., Jenness T., Scott D., Tilanus R. P. J., Economou F., Holland W. S., 2013, *MNRAS*, 430, 2545
 Chapman S. C., Blain A. W., Smail I., Ivison R. J., 2005, *ApJ*, 622, 772

Chapman S. C., Blain A., Ivison R. J., Smail I., Morrison G., 2009, *ApJ*, 691, 560
 Comastri A., Setti G., Zamorani G., Hasinger G., 1995, *A&A*, 296, 1
 Cooray A. et al., 2010, *A&A*, 518, L22
 Coppin K. et al., 2008, *MNRAS*, 384, 1597
 Cowie L. L., Barger A. J., Kneib J.-P., 2002, *AJ*, 123, 2197
 Cutri R. M. et al., 2012, *VizieR Online Data Catalog*, 2311, 0
 Dempsey J. T. et al., 2013, *MNRAS*, 430, 2534
 Dey A. et al., 2008, *ApJ*, 677, 943
 Eisenhardt P. R., Armus L., Hogg D. W., Soifer B. T., Neugebauer G., Werner M. W., 1996, *ApJ*, 461, 72
 Eisenhardt P. R. M. et al., 2012, *ApJ*, 755, 173
 Elbaz D. et al., 2011, *A&A*, 533, A119
 Farrah D. et al., 2001, *MNRAS*, 326, 1333
 Farrah D. et al., 2006, *ApJ*, 641, L17
 Farrah D. et al., 2012, *ApJ*, 745, 178
 Genzel R., Cesarsky C. J., 2000, *ARA&A*, 38, 761
 Genzel R. et al., 1998, *ApJ*, 498, 579
 Gilli R., Comastri A., Hasinger G., 2007, *A&A*, 463, 79
 Goulding A. D., Alexander D. M., Bauer F. E., Forman W. R., Hickox R. C., Jones C., Mullaney J. R., Trichas M., 2012, *ApJ*, 755, 5
 Greve T. R., Ivison R. J., Bertoldi F., Stevens J. A., Dunlop J. S., Lutz D., Carilli C. L., 2004, *MNRAS*, 354, 779
 Hickox R. C. et al., 2012, *MNRAS*, 421, 284
 Hinshaw G. et al., 2009, *ApJS*, 180, 225
 Holland W. S. et al., 2013, *MNRAS*, 430, 2513
 Hopkins P. F., Hernquist L., Cox T. J., Di Matteo T., Robertson B., Springel V., 2006, *ApJS*, 163, 1
 Hopkins P. F., Hernquist L., Cox T. J., Kereš D., 2008, *ApJS*, 175, 356
 Houck J. R. et al., 1984, *ApJ*, 278, L63
 Ivison R. J. et al., 2007, *MNRAS*, 380, 199
 Jarrett T. H. et al., 2011, *ApJ*, 735, 112
 Kovács A., Chapman S. C., Dowell C. D., Blain A. W., Ivison R. J., Smail I., Phillips T. G., 2006, *ApJ*, 650, 592
 Krolak J. H., Begelman M. C., 1988, *ApJ*, 329, 702
 Le Floch E. et al., 2005, *ApJ*, 632, 169
 Lonsdale C. J., Farrah D., Smith H. E., 2006, *Ultraluminous Infrared Galaxies*. Springer-Verlag, Berlin, p. 285
 Lu N., Zhao Y., Xu C. K., Gao Y., GOALS FTS Team, 2013, in Wong T., Ott J., eds, *Proc. IAU Symp. 292, Molecular Gas, Dust, and Star Formation*. Cambridge Univ. Press, Cambridge, p. 249
 Madau P., Ghisellini G., Fabian A. C., 1994, *MNRAS*, 270, L17
 Magnelli B., Elbaz D., Chary R. R., Dickinson M., Le Borgne D., Frayer D. T., Willmer C. N. A., 2009, *A&A*, 496, 57
 Magnelli B. et al., 2012, *A&A*, 539, A155
 Maiolino R., Rieke G. H., 1995, *ApJ*, 454, 95
 Maiolino R., Marconi A., Salvati M., Risaliti G., Severgnini P., Oliva E., La Franca F., Vanzi L., 2001, *A&A*, 365, 28
 Melbourne J. et al., 2012, *AJ*, 143, 125
 Mihos C., 1996, in Murdin P., ed., *Encyclopedia of Astronomy and Astrophysics*. IOP Publishing, Bristol, p. 2413
 Narayanan D. et al., 2010, *MNRAS*, 407, 1701
 Negrello M. et al., 2010, *Science*, 330, 800
 Neugebauer G. et al., 1984, *ApJ*, 278, L1
 Osterbrock D. E., Shaw R. A., 1988, *ApJ*, 327, 89
 Piconcelli E., Cappi M., Bassani L., Di Cocco G., Dadina M., 2003, *A&A*, 412, 689
 Polletta M. d. C. et al., 2006, *ApJ*, 642, 673
 Polletta M. et al., 2007, *ApJ*, 663, 81
 Reddy N. A., Steidel C. C., Pettini M., Adelberger K. L., Shapley A. E., Erb D. K., Dickinson M., 2008, *ApJS*, 175, 48
 Richards G. T. et al., 2006, *AJ*, 131, 2766
 Risaliti G., Maiolino R., Salvati M., 1999, *ApJ*, 522, 157
 Sanders D. B., Mirabel I. F., 1996, *ARA&A*, 34, 749
 Sanders D. B., Soifer B. T., Elias J. H., Madore B. F., Matthews K., Neugebauer G., Scoville N. Z., 1988a, *ApJ*, 325, 74
 Sanders D. B., Soifer B. T., Elias J. H., Neugebauer G., Matthews K., 1988b, *ApJ*, 328, L35

- Schweizer F., 1998, in Kennicutt R. C., Jr, Schweizer F., Barnes J. E., Friedli D., Martinet L., Pfenniger D., eds, Saas-Fee Advanced Course 26: Galaxies: Interactions and Induced Star Formation. Springer-Verlag, Berlin, p. 105
- Scott S. E. et al., 2002, MNRAS, 331, 817
- Scott S. E., Dunlop J. S., Serjeant S., 2006, MNRAS, 370, 1057
- Scott K. S. et al., 2010, MNRAS, 405, 2260
- Scoville N. Z. et al., 2000, AJ, 119, 991
- Smail I., Ivison R. J., Blain A. W., 1997, ApJ, 490, L5
- Soifer B. T. et al., 1984, ApJ, 278, L71
- Solomon P. M., Vanden Bout P. A., 2005, ARA&A, 43, 677
- Spoon H. W. W. et al., 2013, ApJ, 775, 127
- Stern D. et al., 2014, preprint ([arXiv:e-prints](https://arxiv.org/abs/1405.1147))
- Tacconi L. J. et al., 2008, ApJ, 680, 246
- Treister E., Urry C. M., 2005, ApJ, 630, 115
- Tyler K. D. et al., 2009, ApJ, 691, 1846
- Umehata H. et al., 2014, MNRAS, 440, 3462
- Veilleux S., Kim D.-C., Sanders D. B., 2002, ApJS, 143, 315
- Vieira J. D. et al., 2010, ApJ, 719, 763
- Weiß A. et al., 2009, ApJ, 707, 1201
- Williams L. L. R., Lewis G. F., 1996, MNRAS, 281, L35
- Wright E. L. et al., 2010, AJ, 140, 1868
- Wu J. et al., 2012, ApJ, 756, 96
- Wu J. et al., 2014, preprint ([arXiv:1405.1147](https://arxiv.org/abs/1405.1147))

This paper has been typeset from a $\text{\TeX}/\text{\LaTeX}$ file prepared by the author.